From: ACOUSTICAL IMAGING, Vol. 14
Edited by A.J. Berkhout, J. Ridder,
and L.F. van der Wal
(Plenum Publishing Corporation, 1985)

SPATIAL RESOLUTION OF MIGRATION ALGORITHMS

G. Beylkin, M. Oristaglio, and D. Miller

Schlumberger-Doll Research
Old Quarry Road
Ridgefield, CT 06877-4108

ABSTRACT

This paper presents a systematic approach to the description of spatial resolution of seismic experiments and migration (or inversion) algorithms.

We give a brief description of the linearized seismic inverse problem and its solution by migration and inversion algorithms. To consider the spatial resolution at a given point in the medium, we define the domain of coverage in the space of spatial frequencies. This region determines the spatial resolution and is shown to depend on (i) the total domain of integration, which in turn depends on the configuration of sources and receivers and on the frequency band of the signal, and (ii) the mapping of this domain into the spatial frequency domain. This mapping is determined by the background model and can be obtained numerically by ray tracing. Together (i) and (ii) allow us to estimate the limits of spatial resolution at each point in the medium given the configuration of experiment and the background model.

As important examples, we illustrate our approach by considering the spatial resolution of surface seismics and VSP.

INTRODUCTION

Information obtained in seismic experiments is usually finalized in pictures of subsurface structures, a process that is commonly called migration. The question "What do we see in these pictures?" has not been answered fully so far. It is usually understood that what we see is *an image* of the subsurface, more exactly, an image of surfaces of *discontinuities* of the elastic parameters of the medium. For example, various migration algorithms for seismic imaging have been derived over the years by considering such discontinuities as secondary sources [1-13]. Recently, a connection between seismic imaging and generalized Radon transform was made [10]. This result together with the inversion of the generalized Radon transform [14,15] allows to formalize the intuitive point of view that discontinuities are reconstructed via migration algorithms [16].

However, more questions arise. How does the limited aperture of seismic experiments affect the image? How do the initial assumptions of the subsurface structures affect the image? What difference does it make to perform just surface seismic experiments, or just VSP, or both? What would be the configuration of an ideal experiment (though we might not be able to perform it)? All these questions are of crucial importance, since their answers explain what we see in depth sections. All of these questions can, in fact, be formulated as one; namely, what is the spatial resolution of a seismic experiment and migration (or inversion) algorithms and how does it depend on the configuration of the experiment, the reconstruction algorithm and the initial assumptions about the medium?

So far only partial answers are available (see Devaney [17] for example). This paper presents a systematic way of describing the spatial resolution of seismic experiments; that is we give a simple method of estimating the spatial resolution given the configuration of the seismic experiment and the background model. We illustrate our approach by considering limits on spatial resolution of surface seismics and VSP.

1. A MATHEMATICAL FORMULATION OF THE PROBLEM

The problem of nondestructive evaluation in general and of seismic exploration in particular is that of finding parameters of the medium in some region given observations of scattered wave fields on the boundary of that region. Incident wave fields are generated by "point sources" located usually on the boundary of the region. We ignore directional characteristics of real sources in this paper and use δ-function to represent a point source.

The propagation of waves is presumed to be governed by a linear partial differential equation. The specific equation and its coefficients depend on the medium. Here, we consider the simplest equations - the wave equation and the corresponding Helmholtz equation. In this case the medium is described by just one function - index of refraction - which we want to find given a scattered wave field. Similar considerations apply to the elastic equations; however, we restrict ourselves here to the Helmholtz equation for the sake of simplicity.

To formalize what has been said so far, we denote the region of interest by X, its boundary by ∂X, points inside the region X by x, points on the boundary by ξ and η. Let η denote the source positions and ξ the receiver positions. Let the region X be three-dimensional (however, the specific dimension of X is not essential in our approach, and enters only as a parameter). We assume that we are given the function $u(t,\xi,\eta)$ - the scattered field - as a function of time t, source position η, and receiver position ξ. For fixed η and ξ the function $u(t,\xi,\eta)$ is a single seismic trace. We assume that the scattered field is causal

$$u(t,\xi,\eta) = 0, \qquad \text{for} \quad t < 0 \ ,$$

and, thereby, real and imaginary parts of

$$\hat{u}(k,\xi,\eta) = \int_{-\infty}^{+\infty} u(t,\xi,\eta) e^{ikt}\, dt \ . \tag{1.1}$$

satisfy dispersion relations in the frequency domain.

Unfortunately, in seismics neither ξ nor η can be assumed to vary along all of the boundary ∂X. This imposes an important limitation on the spatial resolution. Therefore, we always assume a limited aperture for an experiment and denote parts of the boundary where sources and receivers are located by ∂X_s and ∂X_{rec}, respectively.

Suppose the index of refraction in the region X is of the form

$$n^2(x) = n_0^2(x) + f(x) \ , \tag{1.2}$$

where $n_0(x)$ is known and is usually called the background model. The problem is to characterize the real function $f(x)$ using observations of the scattered field on the boundary ∂X of the region X. If the propagation is governed by the Helmholtz equation, then the scattered field $\hat{u}(k,\xi,\eta)$ satisfies the following integral equation

$$\hat{u}(k,\xi,\eta) = -k^2 \int_X G(k,\xi,x) f(x) v_{total}(k,\eta,x)\, dx \ , \tag{1.3}$$

where G is the Green's function of the background model and v_{total} is the sum of the incident and scattered fields $v_{total} = v_{in} + v$. The Green's function G is the solution of the equation

$$(\nabla_x^2 + k^2 n_0^2) G(k,\xi,x) = \delta(x-\xi) \ ,$$

and, in principle, can be computed given the background model.

We linearize the problem by using instead of (1.3)

$$\hat{u}(k,\xi,\eta) = -k^2 \int_X G(k,\xi,x) f(x) v_{in}(k,\eta,x)\,dx \ . \tag{1.4}$$

This approximation (the so-called distorted wave Born approximation) is usually satisfactory for the singly scattered field. In any case, it can be made arbitrarily accurate by taking the perturbation f to be small enough. We view (1.4) as an equation for the function f. This is an integral equation of the first kind with an oscillatory kernel. Migration and inversion methods provide approximate solutions of this equation.

We assume that the incident field v_{in} is that of a point source at the point η on the boundary ∂X_s and that the source position is fixed. Since (1.4) is a linear integral equation, its solution - which we denote by $f_{est}(x)$ - can be written as

$$f_{est}(x) = 2\,\mathrm{Re} \int_{\partial X_{rec}} \int_0^\infty \hat{M}(k,\xi,\eta,x)\hat{u}(k,\xi,\eta)\,d\xi dk \ , \tag{1.5}$$

with some kernel $\hat{M}$, where $\overline{\hat{M}}(k,\xi,\eta,x) = \hat{M}(-k,\xi,\eta,x)$ and Re denotes the real part of the expression. Equation (1.5) can be rewritten as

$$f_{est}(x) = \int_{\partial X_{rec}} \int_0^\infty M(t,\xi,\eta,x) u(t,\xi,\eta)\,d\xi dt \ , \tag{1.6}$$

using the following relation between two arbitrary real functions g, h and their Fourier transforms $\hat{g}$, $\hat{h}$

$$\int_{-\infty}^{+\infty} g(t)h(t)\,dt = \frac{1}{2\pi} \int_{-\infty}^{+\infty} \overline{\hat{g}}(k)\hat{h}(k)\,dk \ . \tag{1.7}$$

Here,

$$M(t,\xi,\eta,x) = 2\,\mathrm{Re} \int_0^{+\infty} \overline{\hat{M}}(k,\xi,\eta,x) e^{-ikt}\,dk \ , \tag{1.8}$$

and

$$\hat{M}(k,\xi,\eta,x) = \frac{1}{2\pi} \int_{-\infty}^{+\infty} M(t,\xi,\eta,x) e^{-ikt}\,dt \ . \tag{1.9}$$

This paper describes a few possible constructions for the kernel $\hat{M}(k,\xi,\eta,x)$ or $M(t,\xi,\eta,x)$. However, our main concern is to explain to what extent can we recover the function $f(x)$. In other words, what is the relation between $f(x)$ and $f_{est}(x)$.

If the source position is not fixed, then in addition to integrating over all frequencies and receiver positions in (1.5) we can integrate over all source positions along ∂X_s because of the reciprocity between sources and receivers.

We will call the domain of integration $[0,\infty]\times\partial X_{rec}$ (or $[0,\infty]\times\partial X_{rec}\times\partial X_s$ if we have multiple source positions) in (1.5) the *total domain of integration*. In practice, it is always a bounded domain. It is bounded because of limited apertures and bandlimited signals. It is this domain that determines the spatial resolution of reconstructions and the description of "how" is the subject of this paper.

2. ALGORITHMS OF RECONSTRUCTION: MIGRATIONS AND INVERSIONS

Traditionally, an imaging procedure which recovers locations of surfaces of discontinuities was given the name migration, while algorithms aimed to recover the velocity (in our case the function f) were called inversions. Recently developed algorithms [16,18] recover not only the location but also the jump at the discontinuity [19]. Moreover, as can be seen from the example [18], the velocity itself can be recovered in certain situations, since the error appears to be not only smooth, but also small. Thus, the distinction between migrations and inversions becomes blurred.

In any case, a description of a reconstruction algorithm is the description of the kernel $M(t,\xi,\eta,x)$ in (1.6) or $\hat{M}(k,\xi,\eta,x)$ in (1.5). An explicit form of the kernel $M(t,\xi,\eta,x)$ was suggested [16],

$$M(t,\xi,\eta,x) = -\frac{1}{8\pi^2}\,\delta(t-\phi^{out}(x,\xi)-\phi^{in}(x,\eta))\,\frac{1}{A^{out}(x,\xi)A^{in}(x,\eta)}\,h(x,\xi,\eta)\,, \qquad (2.1)$$

or, as it follows from (1.9),

$$\hat{M}(k,\xi,\eta,x) = -\frac{1}{16\pi^3}\,\frac{e^{-ik(\phi^{out}(x,\xi)+\phi^{in}(x,\eta))}}{A^{out}(x,\xi)A^{in}(x,\eta)}\,h(x,\xi,\eta)\,. \qquad (2.2)$$

Here the phase functions $\phi^{out}(x,\xi)$, $\phi^{in}(x,\eta)$ and the amplitudes $A^{out}(x,\xi)$, $A^{in}(x,\eta)$ come from the ray approximation to the Green's functions, namely

$$G^{out}(k,\xi,x) = -A^{out}(x,\xi)e^{ik\phi^{out}(x,\xi)}\,,$$

and

$$G^{in}(k,\eta,x) = -A^{in}(x,\eta)e^{ik\phi^{out}(x,\eta)}\,.$$

The phase functions $\phi^{in}(x,\eta)$ and $\phi^{out}(x,\xi)$ satisfy the eikonal equations

$$(\nabla_x\phi^{in}(x,\eta))^2 = n_0^2(x)\,,$$

and

$$(\nabla_x\phi^{out}(x,\xi))^2 = n_0^2(x)\,.$$

$\phi^{in}(x,\eta)$ is the travel time in the background model from the source located at the point η to the point of reconstruction x inside the region X, and $\phi^{out}(x,\xi)$ is the travel time in the background model from the point of reconstruction x to the receiver located at the point ξ.

Amplitudes A^{in} and A^{out} satisfy the transport equations

$$A^{in}(x,\eta)\,\nabla_x^2\phi^{in}(x,\eta) + 2\nabla_x A^{in}(x,\eta)\cdot\nabla_x\phi^{in}(x,\eta) = 0\,,$$

and

$$A^{out}(x,\xi)\,\nabla_x^2\phi^{out}(x,\xi) + 2\nabla_x A^{out}(x,\xi)\cdot\nabla_x\phi^{out}(x,\xi) = 0\,,$$

along the rays connecting the source location η on the boundary ∂X_s with the point x inside the region X, and the point x with the receiver location ξ on the boundary ∂X_{rec}, respectively.

The function $h(x,\xi,\eta)$ is the Jacobian of a map we will discuss later in the paper. It is easy to compute h (provided we can trace rays in the background model) from the following identity

$$h(x,\xi,\eta)\,d\xi = n_0^3(1+\cos\psi)\,d\omega\,, \qquad (2.3)$$

where

$$\cos\psi(x,\xi,\eta) = \frac{\nabla_x\phi^{out}(x,\xi)\cdot\nabla_x\phi^{in}(x,\eta)}{n_0^2(x)}\,. \qquad (2.4)$$

$\psi(x,\xi,\eta)$ is the angle between the two rays traced from the source and from the receiver to the point x; $d\omega$ is the standard solid angle measure on the unit sphere. Relation (2.3) describes the rate of change at the point x of the direction of the ray connecting point x with the receiver with respect to the receiver position on the boundary ∂X.

The kernel in (2.1) or (2.2) solves the problem of migration for the case of variable background velocity and arbitrary configuration of sources and receivers. The derivation of (2.1) is based on the connection between seismic imaging and generalized Radon transform [10] and the inversion of the Generalized Radon Transform [14,15]. A formal derivation of (2.1) is presented in Ref.16 and a heuristic approach connected with (2.1) in Refs.10,18. Since the reconstruction with this kernel is up to a smooth error, we can replace propagators in (2.1) and (2.2) by any propagators which have the same high frequency asymptotics. Therefore, we can use exact Green's functions and obtain

$$\hat{M}(k,\xi,\eta,x) = -\frac{1}{16\pi^3}\,\frac{\overline{G}(k,\xi,x)}{|G(k,\xi,x)|^2}\,\frac{\overline{G}(k,\eta,x)}{|G(k,\eta,x)|^2}\,h(x,\xi,\eta)\,, \qquad (2.5)$$

and

$$M(t,\xi,\eta,x) = -\frac{1}{8\pi^2}\int_{-\infty}^{+\infty} \bar{G}^{out}(t-\tau,\xi,x)\,\bar{G}^{in}(\tau,\eta,x)d\tau \;\; h(x,\xi,\eta)\,, \tag{2.6}$$

where

$$\bar{G}^{out}(t,\xi,x) = 2\,\mathrm{Re}\int_0^{+\infty} \frac{G(k,\xi,x)}{|G(k,\xi,x)|^2}\, e^{-ikt}\, dk\,, \tag{2.7}$$

and

$$\bar{G}^{in}(t,\eta,x) = 2\,\mathrm{Re}\int_0^{+\infty} \frac{G(k,\eta,x)}{|G(k,\eta,x)|^2}\, e^{-ikt}\, dk\,. \tag{2.8}$$

(2.5) and (2.6) represent another choice of kernels to perform migration.

There are two different physical interpretations of the algorithms depending on the order of integration in (1.5) or (1.6).

i.Integrating over time (or frequency) first, over the receiver positions second.

We illustrate this case using (2.1). Substituting (2.1) into (1.6) we obtain

$$f_{est}(x) = -\frac{1}{8\pi^2}\int_{\partial X_{rec}} u(t,\xi,\eta)\Big|_{t=\phi^{in}(x,\eta)+\phi^{out}(x,\xi)} \frac{1}{A^{out}(x,\xi)A^{in}(x,\eta)}\, h(x,\xi,\eta)\, d\xi\,, \tag{2.9}$$

Here, let us give the following interpretation.

For a given point x (the point of reconstruction), we want to check if there is a reflector at that point. To accomplish this, we go to our data $u(t,\xi,\eta)$ and integrate along the time-distance curve $t=\phi^{in}(x,\eta)+\phi^{out}(x,\xi)$ dictated by the background model. If there were a reflector at the point x then along this curve the data are affected to the greatest extent. The weighting in (2.9) is chosen so that we obtain the jump of the function f at the point x as a result of such an integration.

ii.Integrating over boundary first, over time (or frequency) second.

We obtain using (2.2)

$$f_{est}(x) = -\frac{1}{16\pi^3}\,\mathrm{Re}\int_0^{\infty} \frac{e^{-ik\phi^{in}(x,\eta)}}{A^{in}(x,\eta)} \int_{\partial X_{rec}} \frac{e^{-ik\phi^{out}(x,\xi)}}{A^{out}(x,\xi)}\, h(x,\xi,\eta)\hat{u}(k,\xi,\eta)\, d\xi\, dk\,. \tag{2.10}$$

Using (2.5) we can write still another formula for $f_{est}(x)$,

$$f_{est}(x) = -\frac{1}{16\pi^3}\,\mathrm{Re}\int_0^{\infty} \frac{\bar{G}(k,\eta,x)}{|G(k,\eta,x)|^2} \int_{\partial X_{rec}} \frac{\bar{G}(k,\xi,x)}{|G(k,\xi,x)|^2}\, h(x,\xi,\eta)\hat{u}(k,\xi,\eta)\, d\xi\, dk\,. \tag{2.11}$$

Using (1.7) the corresponding integral in time domain can be written as follows

$$f_{est}(x) = -\frac{1}{8\pi^2}\int_0^{\infty} \bar{G}^{in}(t,\eta,x)\, w(t,\eta,x)\, dt\,, \tag{2.12}$$

where

$$w(t,\eta,x) = \int_0^{\infty}\int_{\partial X_{rec}} \bar{G}^{out}(\tau-t,\xi,x)\, h(x,\xi,\eta)u(\tau,\xi,\eta)\, d\xi\, d\tau\,,$$

Here, we would like to point out the difference in interpretation of (2.9) compared with (2.12). Approach in (2.12) is within the spirit of Claerbout's "full wave" equation migration. However, the propagators we use here differ from those used by Claerbout [3]. This approach can be interpreted as follows.

Taking the scattered field along ∂X (part of the boundary with receivers) we backpropagate this field inside the region X to the point x. We also propagate the incident wave to the point x and then form an integral over time.

It is clear now that (i) and (ii) carry different heuristics. *We note, however, that despite the difference in interpretation, the total domain of integration remain the same in both cases.* This domain of integration was shown [16] to be directly related to the region of coverage in the space of spatial frequences. We discuss it in greater detail in the following section.

3. REGIONS OF COVERAGE IN THE DOMAIN OF SPATIAL FREQUENCIES

Given a function $f(x)$ it can be presented as

$$f(x) = \frac{1}{(2\pi)^3} \int \hat{f}(p) e^{-ip\cdot x}\, dp \ , \tag{3.1}$$

where $\hat{f}(p)$ is the Fourier transform of the function f,

$$\hat{f}(p) = \int f(x) e^{ip\cdot x}\, dx \ .$$

Suppose we restrict the integration in (3.1) to a bounded region D_x, which we call the region of coverage at the point x in the domain of spatial frequences. We have

$$f_{est}(x) = \frac{1}{(2\pi)^3} \int_{D_x} \hat{f}(p) e^{-ip\cdot x}\, dp \ , \tag{3.2}$$

where f_{est} is an estimated value of the function f at the point x. The important feature of this definition of the region of coverage D_x is that we allow the shape of this region to depend on the point of reconstruction x. For real functions f the region of coverage D_x is symmetric with respect to the origin, since in this case $\bar{\hat{f}}(p) = \hat{f}(-p)$ and, therefore, with every point p the region D_x contains also point $-p$.

It was shown [16] that the reconstructed function $f_{est}(x)$ in algorithms in (2.1) and (2.2) is the same one (up to a smooth error, see Figure 1 for an illustration) as in (3.2) provided we describe the region of coverage D_x. *The description of D_x is, in fact, the estimate of spatial resolution.* For a given point x in the medium this description in the ray approximation is given by the following mapping

$$p = k\ \nabla_x (\phi^{out}(x,\xi) + \phi^{in}(x,\eta)) \ , \tag{3.3}$$

where p is a vector in the space of spatial frequences, k is the wave number, ξ is the receiver position and η is the source position and x is the point of reconstruction. The transform in (3.3) maps

$$[\textit{signal frequency band}] \times \partial X_{rec} \times \partial X_s \rightarrow [\textit{space of spatial frequencies}] \ .$$

It maps space of $2n-1$ dimensions into space of n dimensions, where in our case $n=3$. Therefore, we can have a multiple coverage of some parts of D_x. As a general rule, this multiple coverage is used (explicitly or implicitly) for averaging which improves the signal to noise ratio.

This mapping was investigated only with simplifying assumptions. The simplifying assumption [16] is that the Jacobian (the function $h(x,\xi,\eta)$ in (2.3)) of this mapping for a fixed source position is positive. In this case

$$dp = k^2 h(y,\xi,\eta)\, d\xi\, dk \ ,$$

where h is the same as in (2.3) and the mapping (3.3) can be viewed as a change of variables of integration from k,ξ to p. Physically this simplifying assumption means that if a source located at an interior point of X illuminates a region ∂X_{rec} on the boundary, then this region can be smoothly contracted along the rays into a part of a small sphere around the source. This condition is always satisfied in the case of a constant background.

The mapping (3.3) is of a fundamental importance with respect to inversion algorithms. It shows how the total domain of integration (k,ξ,η) on which our data are defined is related to region of coverage in the domain of spatial frequences.

To summarize, the spatial resolution at a given point x defined by the region D_x depends on

i) the total domain of integration, which is determined by the configuration of sources and receivers and the frequency band of the signal, and

ii) the mapping (3.3) of this domain into the domain of spatial frequencies, which is determined by the background model and can be obtained numerically by ray tracing. This mapping is different for each point of reconstruction.

Together (i) and (ii) determine the limits on spatial resolution at each point of reconstruction given the configuration of experiment and the background model.

4. EXAMPLES

We start with Figure 1 which describes what we mean by "smooth error" in reconstructions by migration algorithms. In certain important situations [18], error itself can be small as well.

Figure 2 shows how a box in the total domain of integration is transformed under the mapping (3.3) in the case of a constant background and source-receiver configuration shown in the picture. The source position is fixed and point of reconstruction is the origin. We note that algorithms in (2.1-2.2) and (2.5-2.6) are derived under assumptions of unlimited bandwidth and Figure 2 also illustrates the effect of bandlimiting on the shape of the region of coverage in the domain of spatial frequences. This shape affects the reconstruction and the question how to incorporate the bandlimited nature of the observations to reduce such influence is still unresolved.

We now concentrate on the effects of limited aperture of the experiments. Figure 3 shows a simple single source surface configuration and illustrates the limits imposed on the region of coverage by a limited aperture. These regions are different for different points. In the case of multiple sources certain spatial frequences are covered several times as illustrated in Figure 4. This forms the basis for the CDP method. Indeed, in the case of horizontally layered structures, data corresponding to a common depth point carry information about the p_z component in the domain of spatial frequences.

Figure 5 illustrates the limits imposed on the region of coverage by a limited aperture in an offset VSP. Note that different spatial frequences can be recovered compared to the surface seismics experiments.

Figures 6-12 are adopted from Ref.18; we have added pictures of the regions of coverage in the domain of spatial frequences. Figure 6 shows the configuration of a coincident source-receiver experiment and the data. The scatterers form the shape of the letter "S" in the object area and Figure 7 shows the reconstruction. Note that the coverage of spatial frequences is spherically symmetric and complete. The size of the reconstructed point scatterers depends only on the bandwidth of the signal.

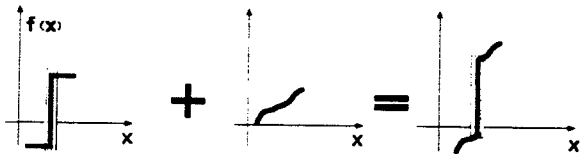

Figure 1. Adding a smooth function changes neither the location nor the size of a jump discontinuity.

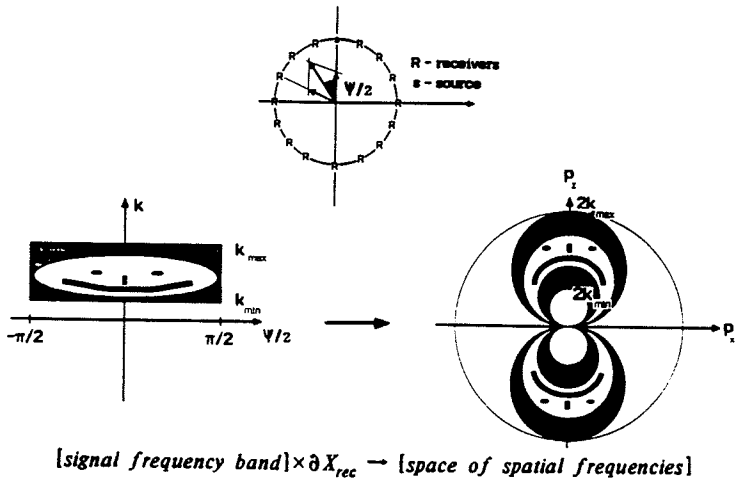

$$[\textit{signal frequency band}] \times \partial X_{rec} \rightarrow [\textit{space of spatial frequencies}]$$

Figure 2. Transformation of a box in the total domain of integration under the mapping in (3.3) in the case of a constant background and source-receiver configuration shown in the top picture.

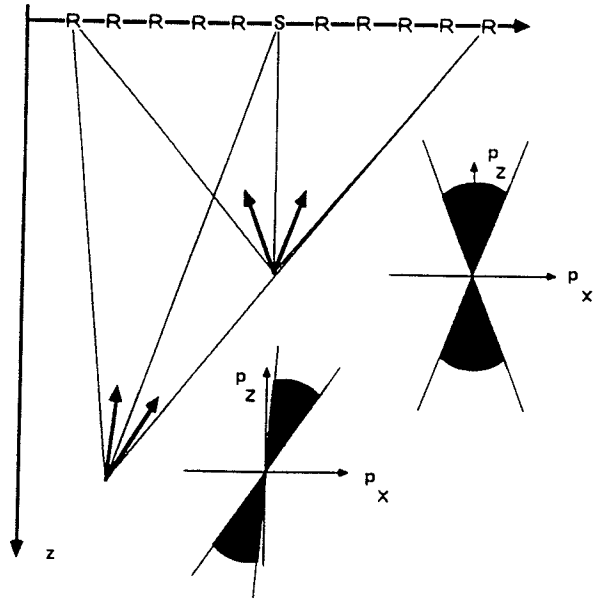

Figure 3. Single source surface seismics configuration. Regions of coverage in the space of spatial frequencies for different points.

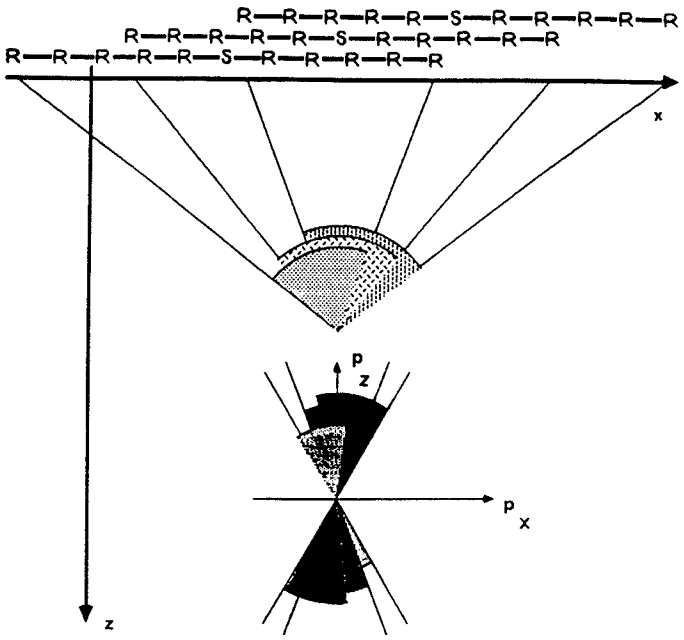

Figure 4. Multiple coverage in the domain of spatial frequencies for a multiple-source configuration.

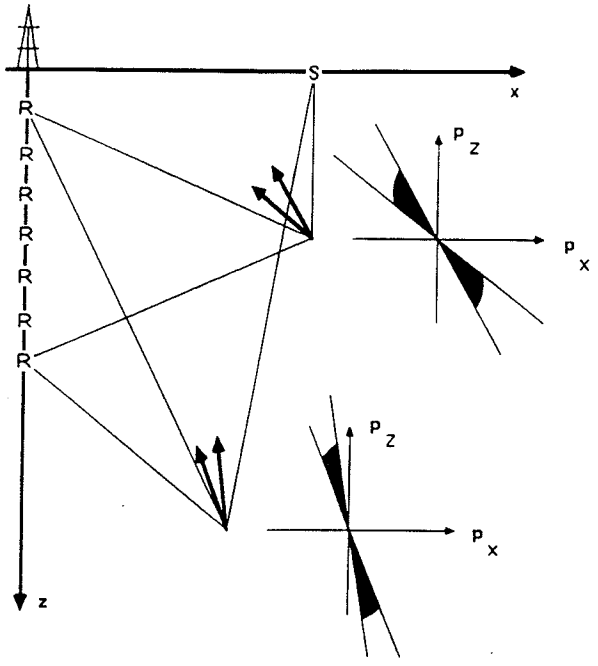

Figure 5. Single source offset VSP configuration. Regions of coverage in the space of spatial frequencies for different points.

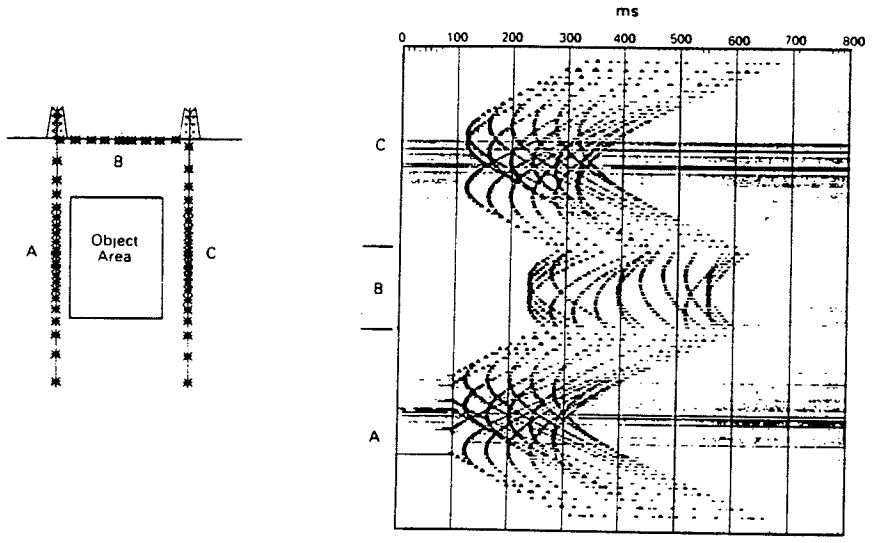

Figure 6. Coincident source-receiver configuration and computer simulated wave field generated by 18 point scatterers of equal strength placed in the medium with constant index of refraction.

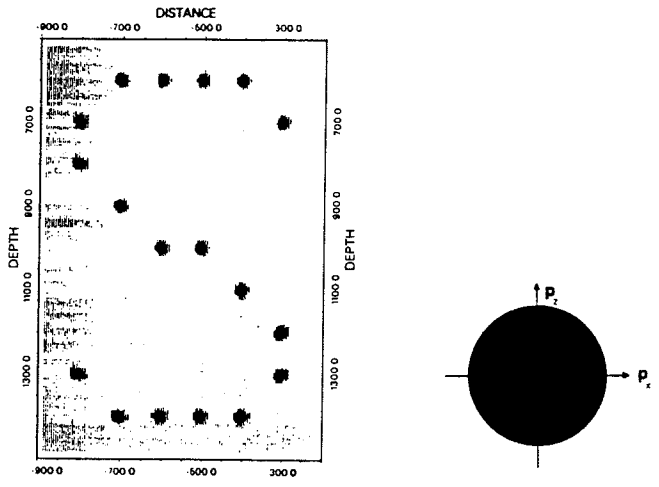

Figure 7. Result of reconstruction using source-receiver configuration and the data shown in Figure 6.

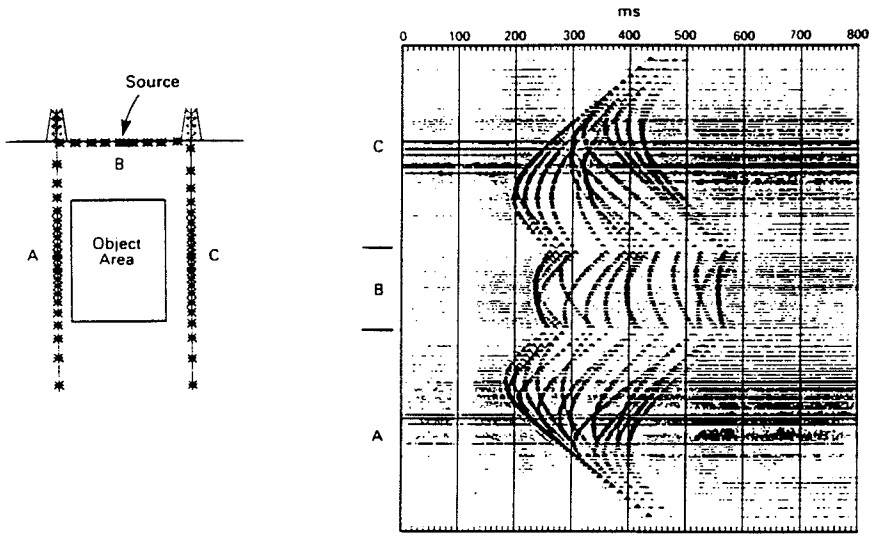

Figure 8. Single source configuration and computer simulated wave field generated by 18 point scatterers of equal strength placed in the medium with constant index of refraction.

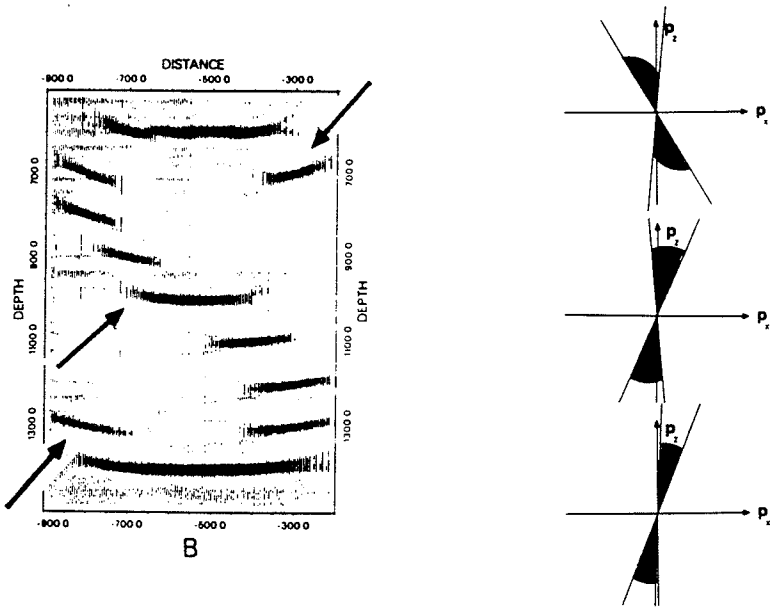

Figure 9. Result of reconstruction and regions of coverage in the space of spatial frequencies for different points. Receivers are located along line B.

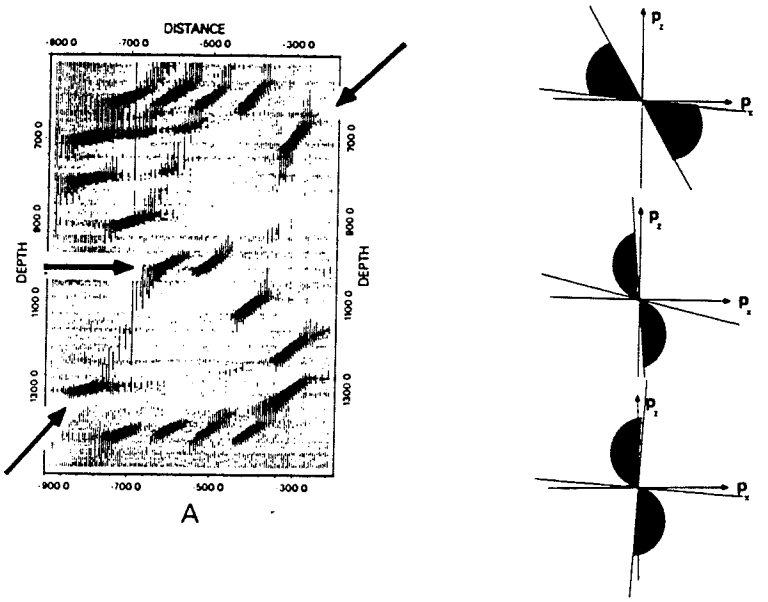

Figure 10. Result of reconstruction and regions of coverage in the space of spatial frequencies for different points. Receivers are located along line A.

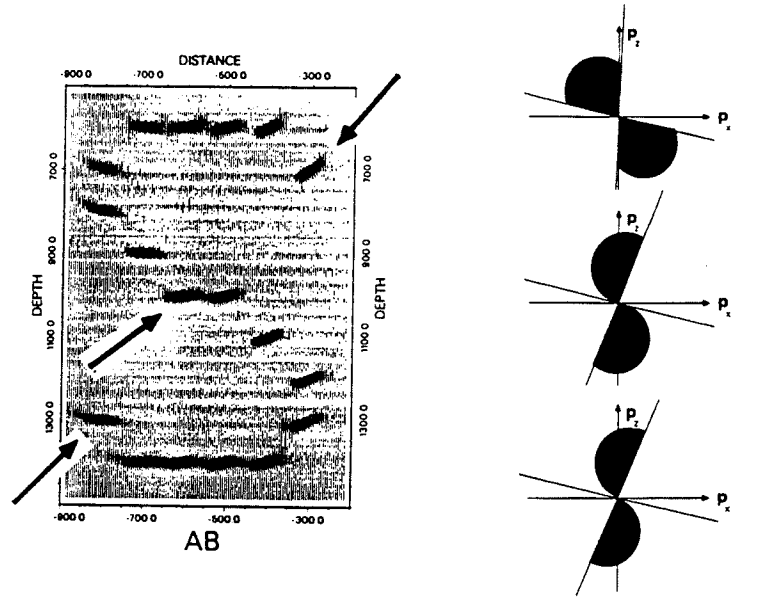

Figure 11. Result of reconstruction and regions of coverage in the space of spatial frequencies for different points. Receivers are located along lines AB.

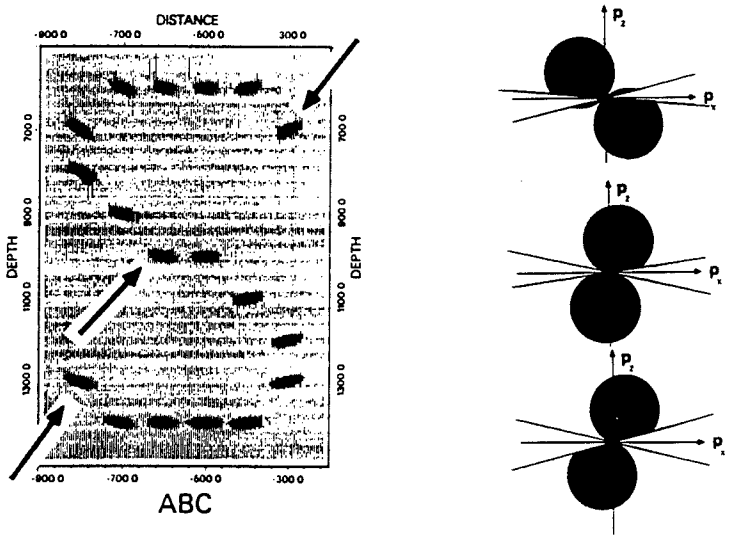

Figure 12. Result of reconstruction and regions of coverage in the space of spatial frequencies for different points. Receivers are located along lines ABC.

Figure 8 shows the configuration of a single source experiment and the data. Figure 9 shows the reconstruction using data collected on the surface. Pictures on the right illustrate limits on the region of coverage caused by a limited aperture at different points. Note poor resolution in the horizontal direction (p_x component). Figure 10 shows the reconstruction and limits on regions of coverage in the offset VSP type of experiment. Note the difference in coverage between Figure 9 and 10 and the effects on the image. Figure 11 shows the reconstruction in combined surface-seismics-VSP experiment. The effects of a limited aperture are present, but one can also see the influence of the bandlimited signal on resolution in different directions (see Figure 2). Figure 12 shows the reconstruction using all the data in the experiment of Figure 8. Here limited aperture effects are minimal. Despite a noticeable influence of the bandlimited signal on resolution in different directions, the reconstruction is almost perfect.

REFERENCES

1. Hagedoorn, J.G., A process of seismic reflection interpretation, Geophysical Prospecting , v.2, 85:127 (1954).
2. Claerbout, J. F., Toward a unified theory of reflector mapping, Geophysics, v. 36, 467:481 (1971).
3. Claerbout, J., "Fundamentals of geophysical data processing", McGraw-Hill, New York, (1976).
4. French, W.S., Two-dimensional and three-dimensional migration of model-experiment reflection profiles, Geophysics, v. 39, 265:277 (1974).
5. Schneider, W. A., Integral formulation for migration in two and three dimensions,Geophysics, v. 43, 49:76 (1978).
6. Stolt, R. M., Migration by Fourier Transform, Geophysics, v. 43, 23:48 (1978).
7. Cohen, J. K. and Bleistein, N., Velocity inversion procedure for acoustic waves, Geophysics, v. 44, 1077:1085 (1979).

8. Berkhout, A. J.,"Seismic migration", Elsevier, Amsterdam/New York, (1980).

9. Norton, S. G., Linzer, M., Ultrasonic reflectivity imaging in three dimensions: Exact inverse scattering solutions for plane, cylindrical, and spherical apertures, IEEE Trans. on Biomedical Engineering, v. BME-28, No. 2, 202:220 (1981).

10. Miller, D. E., Integral transforms and the migration of multiple-offset borehole seismic profiles, SDR Research Note, December 1983.

11. Gelchinsky, B., Ray Asymptotic Migration (Basic Concepts), in Expanded Abstracts of 53rd SEG Meeting, Society of Exploration Geophysics, Las Vegas, 385:387, (1983).

12. Carter, J.A., Fraser L.N., Accommodating lateral velocity changes in Kirchhoff migration by means of Fermat's principle, Geophysics, v.49, 46:53, (1984).

13. Rose, J.H., Exterior reconstruction of a three dimensional scatterer, Wave Motion, 6, 149:154, 1984

14. Beylkin, G., "Generalized Radon transform and its applications", Ph.D. thesis, NYU, (1982).

15. Beylkin, G., The inversion problem and applications of the generalized Radon Transform, Comm. Pure Appl. Math., v. 37, 5, 579:599, (1984).

16. Beylkin, G., Imaging of Discontinuities in the Inverse Scattering Problem by Inversion of a Causal Generalized Radon Transform, J. Math. Phys., 26, 99:108 (1985).

17. Devaney, A.J., Geophysical Diffraction Tomography, IEEE Trans. on Geoscience and Remote Sensing, vol.GE-22, 1, (1984).

18. Miller, D., Oristaglio, M., Beylkin, G., A new formalism and old heuristic for seismic migration, in Expanded Abstracts of 54th SEG Meeting, Society of Exploration Geophysics, Atlanta, 704:707, (1984).

19. Beylkin, G., Reconstructing discontinuities in multidimensional inverse scattering problems: smooth errors versus small errrors, to appear, Special issue of Applied Optics on Industrial Applications of Computed Tomography and NMR Imaging, May 1985.